**Article:**
Glover, ZJ, Francis, MJ, Bisgaard, AH et al. (2020) Dynamic moisture loss explored through quantitative super-resolution microscopy, spatial micro-viscosity and macroscopic analyses in acid milk gels. Food Hydrocolloids, 101. 105501. ISSN: 0268-005X

https://doi.org/10.1016/j.foodhyd.2019.105501

# Dynamic moisture loss explored through quantitative super-resolution microscopy, spatial micro-viscosity and macroscopic analyses in acid milk gels

Zachary J. Glover[a,b,*], Mathew J. Francis[b], Anne Højmark Bisgaard[a], Ulf Andersen[c], Lene Buhelt Johansen[c], Megan J. Povey[b], Melvin J. Holmes[b], Jonathan R. Brewer[d], Adam Cohen Simonsen[a]

[a] *Department of Physics, Chemistry and Pharmacy, University of Southern Denmark,Campusvej 55,5230 Odense, Denmark*
[b] *School of Food Science and Nutrition, University of Leeds,LS2 9JT, UK*
[c] *Arla Foods a.m.b.a, Agro Food Park 19, 8200 Aarhus, Denmark*
[d] *Department of Biochemistry and Molecular Biology,University of Southern Denmark,Campusvej 55,5230 Odense, Denmark*

**Abstract**

Molecular interactions and dynamic changes at a range of length scales affect the structuring of food materials, as such it is essential to explore structure at a range of different length scales. Herein, four acid milk gel samples are produced from either fresh or reconstituted skim milk that either had no heat treatment or had undergone heat treatment at 85 °C for 10 minutes. Milk acid gels demonstrate complex structure on a range of length scales of interest in colloidal materials and exhibit different macroscopic and water binding properties. A method is presented to measure the dynamic moisture loss in these samples, without applying external force. Super-resolution microscopy images are quantitatively analysed to describe the gel microstructure with

*Corresponding author
*Email addresses:* glover@sdu.dk (Zachary J. Glover), adam@memphys.sdu.dk (Adam Cohen Simonsen)

precise features. Fluorescent Lifetime Imaging Microscopy is used to spatially resolve differences in molecular confinement across the sample's microstructure, which is quantified for each sample. Moisture loss and microstructural analyses are correlated to bulk and macroscopic properties determined through rheological and texture analysis, pH and conductivity measurements. More severe thermal and processing treatments leads to a reduction in moisture loss over time. Differences in moisture loss and mechanical properties relate to different thermal processing histories, but are not fully explained by levels of denatured whey proteins, and appear related to changes in mineral balance. The methods presented provide a comprehensive and complementary overview of material properties across relevant length scales and relevant sample conditions.

*Keywords:* Super-resolution (STED) microscopy, Fluorescent Lifetime Imaging Microscopy (FLIM), Dynamic moisture loss, Spatially resolved micro-viscosity, 2D spatial correlation analysis

---

## 1. Introduction

There are many physical properties of a food material that might affect its organoleptic qualities which may be altered during processing and storage to the point of consumption, from during handling and production through to consumption. Consumers are most familiar with certain expected macroscopic behaviours of a food, such as the taste, texture, creaminess, bite or mouthfeel (Laguna, Farrell, Bryant, Morina, and Sarkar, 2017). Consumer expectations vary between food categories and across regional markets, for example whether or not one should expect to have to shake a separated salad dressing or chocolate milk before consumption, through to the acceptable level of syneresis one might find on top of a fermented dairy product. Such macroscopic behaviours are governed by interactions on the colloidal scale. It is non-trivial to relate or predict the behaviour of a material on one length scale, based on measurements conducted at another, therefore, a wide range of quantitative analytical tools are required. There is a growing toolkit of analytical techniques available to the food scientist that are capable of probing the nano and micro scale of food structures which can provide both novel insights and levels of quantification about the colloidal regime that has not previously been possible (Mezzenga, Schurtenberger, Burbidge, and Michel, 2005). Investigations into the microstructure must be closely matched to relevant macroscopic analyses to build an understanding of how behaviours on different length scales relate to the overall properties of a product (Krop, Hetherington, Holmes, Miquel, and Sarkar, 2019). With the emergence of novel technologies and big data processing these new methods may offer rapid screening tools for sample and product optimisation and

allow for data-backed objective decision making.

An area where such emergent technologies have potential application is within recombined dairy products (AlKanhal, Abu-Lehia, and Al-Saleh, 1994). Currently, there is an awareness within the dairy industry and with dairy researchers that products made from exclusively recombined powders have altered product qualities to their fresh equivalents. Changes in mechanical properties due to heating (Lucey, Tamehana, Singh, and Munro, 1998b) and whether produced from fresh or reconstituted milk (Glover, Ersch, Andersen, Holmes, Povey, Brewer, and Simonsen, 2019b) have previously been shown. In order to study this effectively, methods are required that can characterise the various physical properties of interest, and then seek to quantify the differences between them. Methods of characterisation and quantification can provide tools to minimise differences between recombined and fresh products and capitalise on the novel product properties that could be achieved from different raw materials and processing.

One important quality parameter in fermented dairy products is the moisture binding capacity of a gel (Amatayakul, Sherkat, and Shah, 2006). A high level of syneresis may be undesirable in a yoghurt or cream cheese product (Loveday, Sarkar, and Singh, 2013) but the ability to control the release of moisture at the correct rate is essential in cheese making, not only for generating the correct curd texture, but for process efficiency.

Other physical properties are important for the quality of fermented dairy products, which can be investigated on the macro scale with rheometry and texture analysis. It has been shown that there is not a simple relationship between moisture holding and rheological properties, the explanation to which

in soy protein and whey protein gels has been shown to relate to the coarseness of the microstructure, interpreted as the size of the features in the gel, (Urbonaite, De Jongh, Van Der Linden, and Pouvreau, 2015; Urbonaite, van der Kaaij, de Jongh, Scholten, Ako, van der Linden, and Pouvreau, 2016). Controlling the coarseness of the gels, can allow the water binding to be optimised. Therefore, the ability to measure and quantify gel morphology will be an advantage in understanding water binding.

Whey proteins play an important role in texture formation and water binding in certain fermented dairy products. In yoghurt manufacturing it is known that pre-heating the milk prior to fermentation causes denaturation of $\beta$-lactoglobulin ($\beta$-lg) (Lucey, Munro, and Singh, 1999). Whilst it is the caseins that contribute to network formation under acidification, denatured $\beta$-lg can covalently bind to $\kappa$-casein, which is present at the surface of casein micelles, and natively provides electrostatic and steric stability to the micelles. Both the $\kappa$-casein and the $\beta$-lg have a free thiol group, which is exposed in the denatured $\beta$-lg which can then covalently bind to the $\kappa$-casein at the surface of the micelle (Corredig and Dalgleish, 1996; Nair, Dalgleish, and Corredig, 2013; van Vliet, Lakemond, and Visschers, 2004; Vasbinder, Alting, Visschers, and de Kruif, 2003). The presence of $\beta$-lg increases the water holding capacity of the gel and the body of the final product, maximising the potential of the raw ingredient. Without heating the $\beta$-lg would remain in the serum phase and be less interacting. It is of interest to understand how the presence of $\beta$-lg contributes to the microstructure of a dairy gel as well as its macroscopic properties, and how its effects may be mitigated or maximised in recombined products where a degree of denaturation is likely

to have occurred due to the pre-concentration and drying processes involved in powder manufacture (Lucey et al., 1998b).

Confocal microscopy has been widely used in the assessment of dairy and food microstructures (Lucey, Munro, and Singh, 1998a; Lucey, Teo, Munro, and Singh, 1998c; Auty, Twomey, Guinee, and Mulvihill, 2001; Auty, O'Kennedy, Allan-Wojtas, and Mulvihill, 2005). Super-resolution microscopy offers the potential to observe colloidal structures on a smaller length scale, that have not previously been possible, these smaller length scales are of absolute relevance to colloidal interactions. Stimulated Emission Depletion (STED) microscopy, a super-resolution technique, is based on a confocal set up, and utilises a second laser, which overlays with the excitation beam in a torus shape. The second beam causes stimulated depletion of the fluorophores it interacts with, the emitted light from which can be filtered out. Therefore, light is collected from a smaller area and the image has greater resolution (Hell and Wichmann, 1994; Hell, 2003; Hell, 2008; Busko, Baluschev, Crespy, Turshatov, and Landfester, 2012).

STED has proven to be an effective tool for monitoring the microstructures in dairy products containing a protein network, with and without embedded fat droplets (Glover et al., 2019a). It has been demonstrated using label free Coherent Anti-Stokes Raman Scattering (CARS) microscopy that STED imaging can be performed with a dye that does not affect the final microstructure of a milk gel (Glover et al., 2019b).

By coupling super-resolution imaging with quantitative autocorrelation based image analysis it has been possible to differentiate samples based on whether formed from fresh or reconstituted skim milk, and with gelation in-

duced by acid or rennet, where samples exhibiting differences in microstructure have been shown to have different rheological properties. (Glover et al., 2019b). Cross-correlation analysis has been utilised for images with two different channels to assess relative distributions of fat and protein, able to determine the separation distance between a fat droplet and the protein network it is embedded within (Glover et al., 2019a).

The potential for the use of molecular rotary probes in foods to sense the local viscosity and water activity has previously been explored (Ludescher, Peting, Hudson, and Hudson, 1987; Haidekker and Theodorakis, 2007) and reviewed (Strasburg and Ludescher, 1995; Alhassawi, Corradini, Rogers, and Ludescher, 2018). These measurements could provide a novel tool for monitoring a product over its lifetime, especially if intrinsic probes can be utilised. Fluorescence Lifetime Imaging Microscopy (FLIM) offers a tool to spatially resolve the fluorescent lifetime of a rotary probe and gain localised information on the molecular mobility and confinement across a samples microstructure. FLIM imaging has been utilised in many biological samples, but as of yet it has not been fully exploited within food science (Kuimova, Yahioglu, Levitt, and Suhling, 2008; Kuimova, Botchway, Parker, Balaz, Collins, Anderson, Suhling, and Ogilby, 2009; Levitt, Kuimova, Yahioglu, Chung, Suhling, and Phillips, 2009; Kuimova, 2012). FLIM measurements can be used to obtain spatially resolved information on physical and chemical properties such as local viscosity and ion concentrations.

In this study four acid milk gel samples were prepared from fresh or reconstituted milk, having either no heat treatment, or a pre-heat treatment of 85 °C for 10 minutes, equivalent to that used in yoghurt manufacture.

The samples under investigation were chosen to discern whether differences in structures produced fresh or reconstituted milk were primarily due to the thermal load placed upon the milk during concentration and drying, and whether further heating upon reconstitution reduced or increased these differences. Acid milk gels have been characterised with a range of macroscopic methods, such as rheology, texture analysis, bulk pH and conductivity measurements including a novel protocol to measure the dynamic moisture loss of a gel under gravity. The macroscopic properties have been compared to microstructural analyses of super-resolution STED images, capable of discerning the typical length of the protein domains, inter-pore distance and fractal dimension. FLIM imaging has been used to spatially resolve where the molecular movement of the aqueous phase is confined in the gel network. Cross-correlation and image analyses have been used to quantify the area in each image that the mobility of water is affected by the presence of the protein network, which is characteristic for the gel samples. An ensemble of analytical techniques has been applied to provide a detailed insight into the physical properties of milk gels at different, relevant length scales. The combination of analytical techniques provides a greater understanding of the effects of thermal and processing treatments on the final physical properties of the gel. Characterisation occurs at three distinct scales, from the chemical behaviour, pH, conductivity and levels of denatured whey protein, to the nano/micro scale by quantifying the physical structures their interaction with the aqueous. The chemical and micro scale information is related to the overall macroscopic properties of the gel, allowing parameters relevant to a food's quality to be better understood.

## 2. Materials & Methods

### *2.1. Sample preparation*

Four acid induced skim milk gels were prepared, from fresh or reconstituted skim milk having undergone no heat treatment or a heat treatment of 85 °C for 10 minutes, as would be typical in the production of a yoghurt. Fresh milk was locally purchased (Arla Foods a.m.b.a. U.K. / Denmark). Reconstituted milk was prepared with 12 % (w/w) skim milk powder (Arla Food a.m.b.a, Denmark) in water purified with a Milli Q system (Millipore, Bedford, UK) to the same solids content as fresh skim milk (Lucey et al., 1998c). These samples were stirred using a magnetic stirrer for 30 minutes, and left to rehydrate in the fridge for 24 hours to allow full rehydration of the milk proteins. Samples undergoing heat treatment were batch heated in a container in a water bath until reaching 85 °C, this temperature was maintained for 10 minutes before cooling in container under running cold water and refrigerating before use. In all cases acid gels were produced using 2.8 % of Glucono-$\delta$-Lactone (GDL)(Sigma-Aldrich, USA), stirring by hand or tube inversion for one minute to disperse the GDL prior to incubating at 35 °C for 90 minutes. Prior to acidification the samples are complex concentrated dispersions containing protein, lactose, small level of fat and minerals. Following acidification, the dominant protein, the caseins, will come out of solution, and the serum phase will contain the proteins that do not form the network, any non-incorporated fat, the lactose and soluble minerals.

### *2.2. STED imaging*

The milk protein was stained for STED imaging by adding dye to acidified milk. 0.28 g GDL was added to 10 ml of milk, which was inverted by hand for one minute. 600 $\mu$l of milk was then sampled to which 3 $\mu$l of Atto 488 NHS-Ester (Atto-Tec GmbH, Siegen, Germany), dissolved in DMSO (99.9 % pure, Sigma-Aldrich) was added to give a final concentration of 510 $\mu$M in the milk. This stained sample was transferred to a $\mu$-Slide 8 Well chamber (ibidi, Germany), and incubated at 35 °C for 90 minutes before imaging. Samples were prepared in triplicate and three gels were produced from each replicate, 12 images were taken per gel (n=108).

Imaging was performed using a Leica TSC SP8 STED microscope (Leica Gmbh, Mannheim, Germany). A single excitation channel utilised a pulsed white light laser at 488 nm, with detection using a gated hybrid detector (0.3 -6 ns) between 500 - 560 nm. The STED depletion beam was set to a wavelength of 592 nm. The pixel size was optimised for STED imaging at 29.88 nm, 2.10 X zoom was used to give a final image of 1856 x 1856 pixels equivalent to 55.3 $\mu m^2$. A HCX PL AP 100X/1.40 OIL STED objective was used. Images were taken $> 7$ $\mu$m away from the glass interface to avoid anomalies in gel formation at the glass interface. Atto 488 NHS has been demonstrated to be appropriate for imaging milk gel samples previously, using label free CARS microscopy as a negative control to demonstrate that the structures in the gel were not affected by the presence of the dye (Glover et al., 2019b).

| | Fresh skim milk | Reconstituted skim milk |
|---|---|---|
| No Heating | FSM | RSM |
| Heated (85 °C 10 min) | FHSM | RHSM |

Table 1: Table showing sample reference codes for the four different sample preparations investigated

### *2.3. FLIM Measurements*

Fluorescent Lifetime Imaging Microscopy (FLIM) measurements were conducted on the four acid milk gel samples using the probe Viscous Aqua (Ursa Bioscience, MD, U.S.A.). The probe was diluted in MilliQ water as per the manufacturers instructions and added to acidified milk in the same manner described above for the STED imaging. Samples were prepared in triplicate, with two gels being produced from each sample, and 10 images taken per gel (n=60).

Imaging was conducted using a customised Nikon microscope capable of multiphoton excitation and STED equipped with a Becker & Hickl FLIM system. A Nikon Plan Apo IR 60x/1.27 water objective and Hybrid Photo Detectors (HPD100 from Becker & Hickl GmbH, Germany) and SPC-150 TCSPC Modules (Becker & Hickl GmbH, Germany) were used for collecting the data. Excitation was conducted using a Mai Tai DeepSee Ti:Sapphire oscillator at 850 nm, a long pass filter was used to collect light above 460 nm in a single channel. Imaging was performed with SPCM software (Becker & Hickl, GmbH, Germany). Images were 256x256 pixels with 1024 time bins per pixel, pixel size was 250 nm producing and image equivalent to 60 $\mu m^2$ Imaging was conducted until there were 1300 lifetime counts in the me-

dian pixel. Images were processed using SPCImage (Becker & Hickl GmbH, Berlin, Germany). The fluorescent lifetime in each pixel was determined using a two component exponential model. Lifetime images were produced using a moving bin level of 4, giving an area of 7x7 pixels. Lifetime fitting gave an output of two lifetime values and their relative contributions, from which a weighted mean lifetime image was generated in MATLAB (Mathworks, U.S.A.). Intensity images were produced based on the total photon count in each pixel.

The fluorescent lifetime, $\tau_f$, can be related to viscosity as follows (Kuimova, 2012):

$$\tau_f = \frac{z\eta^{\alpha}}{k_r} \tag{1}$$

$$\log \tau_f = \log(\frac{z}{k_r}) + \alpha \log \eta \tag{2}$$

where $\eta$ is the viscosity and $z$ and $\alpha$ are constants and $k_r$ is a radiative decay constant. The relationship shown in equations 1-2 can be used to equate fluorescent lifetime measurements to viscosity, whether in bulk or when spatially resolved. This is the basis of interpreting the FLIM images, where differences in fluorescent lifetime can be seen in different regions of a gel's microstructure.

### *2.4. Image Analysis*

2D spatial auto and cross correlation analyses were performed on the STED and FLIM images respectively. The STED images were analysed with autocorrelation analysis as per Glover et al. (2019b). FLIM images were

analysed with a cross correlation method based upon Glover et al., (2019a) and fit with a model presented by Ako, Durand, Nicolai, and Becu (2009).

The normalised autocorrelation (one input image) and cross-correlation (two input images) images can be determined as shown in equation 3. Normalisation and mean subtraction can remove variation in pixel intensity originating from the acquisition system and translate the data to oscillate around zero, aiding data interpretation.

$$c(a,b) = \frac{\mathcal{F}^{-1}[\mathcal{F}(I_1 - \langle I_1 \rangle) \cdot \mathcal{F}^{*}(I_2 - \langle I_2 \rangle)]}{\sigma_{I1} \cdot \sigma_{I2}} \tag{3}$$

$c(a,b)$ is the normalised cross-correlation image, $\mathcal{F}^{-1}$ is the inverse Fourier transform, $\mathcal{F}$ is the Fourier transform, $\sigma_{I1}$ is the standard deviation of the intensity values across Image 1, $I_1$, and $\sigma_{I2}$ is the standard deviation of the intensity values across Image 2, $I_2$. Angular brackets indicate the average intensity in the images.

Two stretched exponential models have been used previously to extract information from radially averaged correlation images. The first, described by Ako et al. (2009) has been applied in this case to determine the typical decay length in the cross-correlation image generated from the fluorescent lifetime image and corresponding intensity image, shown in equation 4. The second model, described by Glover et al. (2019b) has been applied to STED microscopy images of the acid gel network and has been used to extract the typical size of the protein domains and the inter-pore distance, shown in

equation 5.

$$p(r) = C \cdot e^{-(\frac{r}{\xi})^{\beta}} \tag{4}$$

$$p(r) = C \cdot e^{-(\frac{r}{\xi})^{\beta}} \cdot \cos(\frac{2\pi(r - r_1)}{\lambda}) \tag{5}$$

The models in equations 4 and 5 are fitted to the radial distribution of the correlation images using the MATLAB minimisation function *'fmincon'*, where $r$ is the initial radial distance and $r_1$ is the displaced radial distance. In both equations 4 and 5, $\xi$ represents the short order characteristic length scale. In equation 5, $\lambda$ corresponds to the longer order characteristic length scale in the STED images.

The Fractal Dimension is calculated from the radially averaged power spectrum decay as described previously (Glover et al., 2019b; Super and Bovik, 1991; Marangoni, Acevedo, Maleky, Peyronel, Mazzanti, Quinn, Pink, et al., 2012).

### *2.5. Dynamic Moisture Loss*

An experimental setup was conceived to monitor the moisture loss from a sample over time where the driving forces for moisture expulsion were minimised. Acid milk gels were formed from the four milk sample under investigation using GDL as described above. 35 ml of acidified milk was transferred to a sieve that had been tightly wrapped in foil on its underside.

The sieve was covered to prevent evaporative losses and then incubated at 35 °C for 90 minutes. Following incubation the foil was removed on the underside and the top surface left covered. The sieve was suspended over a 100 ml beaker on top of a balance. The mass was noted every 30 seconds for the first 5 minutes and every minute thereafter up to 30 minutes. The initial weights of the sieve, beaker, foil, and milk added were all noted and used to determine the cumulative moisture loss from each sample over time. Samples were run in triplicate.

### *2.6. Rheometry*

A Kinexus Ultra Rheometer (Malvern Instruments, Worcestershire, UK) was used to measure the rheological properties of the four acid milk gels. The rheometer was operated using the rSpace software. The rheometer was used in a bob and cup setup using a Peltier Cylinder cartridge with a C25 vane tool. The lower geometry was set to 35 °C for all experiments. Samples were added immediately following addition of GDL, prepared in the same way as described above. Silicon oil (VWR Chemicals, PA, U.S.A.) was added to the rim of the rheometer plate to prevent evaporation, before being enclosed with a lid. A single frequency setting was used over time for 90 minutes, with a frequency of 1 Hz at 1 % shear strain with data logging every 10 seconds, followed by a frequency sweep between 1 - 400 Hz with 20 intervals per decade to determine the yield strain and stress of the gel that had formed. One-way ANOVA with post-hoc Tukey's honestly significant difference tests were performed using MATLAB on the final rheological parameters after 90 minutes. Data was plotted from the gel point, defined as when the tan$\delta$ dropped below 45 °. Samples were run in triplicate.

### *2.7. Texture Analysis*

The Young's modulus of the four acid skim milk gel samples was determined using a TA.XT Plus Texture Analyser (Stable Microsystems, Godalming, U.K.). Gels were produced by acidifying the milk samples as described above, and placing 50 ml of milk into individual round plastic containers, before incubating at 35 °C for 90 minutes. Gels were assessed immediately following incubation. The gels were measured with a compression test using a 45 mm diameter disc probe from a back extrusion rig, with a pre-test speed of 3, test speed of 3 mm/s and post test speed of 2 mm/s, to a distance of 2.5 mm with triggering set to an force of 4 g. This gave a sufficient surface area to trigger the system and produce a measurement. The Young's modulus was determined based on the initial gradient of the stress vs strain curve whilst it was in a linear regime. Samples were prepared in triplicate, and three gels were produced from each replicate (n=9).

### *2.8. pH and Conductivity*

The pH and conductivity of the samples were measured using an Orion Star A215 pH/Conductivity meter (Thermo Scientific, MA, U.S.A.). The final pH of the gel samples was measured on the samples following texture analysis (n=9). The conductivity of the acid skim milk gels was measured during acidification. Batches of each sample type were prepared, and acidified with GDL and split into falcon tubes to have one sample to measure every 10 minutes from 0 to 90 minutes. In this way samples were only measured once, as making a probe measurement during gelation would disrupt or destroy the forming gel. A reference sample was taken before acidification. Sample series were prepared in triplicate.

### *2.9. Protein Chemical Analysis*

The protein composition, including relative amounts of denatured $\beta$ -lg was determined using LC-TOF. Native $\beta$ -lg is considered as the $\beta$ -lg that is soluble at pH 4.55. Samples were prepared by taking 15 ml of the milk samples, adding 5 ml 0.4M Na3-citrate and stirring for 30 minutes, before adjusting the pH to 4.55. Samples were analysed without pH adjustment to measure the total content of whey protein, including the non-native proteins. Samples were then centrifuged at 10,000 RPM for 10 minutes before sampling 200 $\mu$l of supernatant. 1 ml of reduction buffer (100 mM Na3-citrate; 6 M Urea) and 20 $\mu$l of 1 M DTE was added. Samples were mixed and incubated for 60 min at 37 °C. After incubation, the samples were centrifuged at 10,000 rpm at 5 °C for 10 min. 200 $\mu$l of the supernatant was transferred to a vial and analysed using an Infinity II LC Systems LC- TOF (Agilent Technologies, CA, U.S.A.). LC-TOF was run on a Poroshell 120 SB-C18 2.1x5 mm 2.7 Micron + Guard Column (Agilent) at 40 °C. Mobile phase A was 0.1 % TFA in water, mobile phase B was 0.1 % TFA in MeCN. A gradient of 0-34 B % from 0 - 12 minutes and 34 - 46.5 B % from 12 - 28 minutes was used, with a flow of 0.35 ml/min and an injection volume of 8 $\mu$l and a UV wavelength of 214 nm. The whey proteins are identified by molecular mass, where genetic variant $\beta$-lg A is 18.367 Da and genetic variant $\beta$-lg B is 18.281 Da.

### *2.10. Statistical analysis*

Pair-wise comparisons between variables were conducted for each variable using a One-way ANOVA with post-hoc Tukey's honestly significant difference tests were performed using MATLAB, results were considered statistically significant for $p<0.05$. The degree of correlation between different

variables was assessed by determined the correlation coefficients using the MATALAB function *'corrcoef'*. Correlation between variables was considered above a coefficient level of 0.9, where strong correlation was considered above values of 0.98.

## 3. Results & Discussion

### *3.1. Microscopy Images*

Figure 1 shows representative STED microscopy images of four acid skim milk gels, produced from either fresh or reconstituted skim milk, having had no heat treatment or having undergone heat treatment. The resolution obtained using STED allows structures to be resolved below the diffraction limit of light, to under 100 nm, on the order of a single casein micelle. It is non-trivial to qualitatively describe and discriminate the types of structure seen in these images, however some morphological differences can be seen between the FSM samples (figure 1a) and the other three samples which have undergone more extensive thermal processing (figures 1b-d). The structures in the FHSM, RSM and RHSM all appear to have longer, thinner strands in the gel network in comparison to the FSM sample. In order to qualify subjective observations and to assess whether differences in microstructure relate to differences in macroscopic behaviour, quantification is required. Quantitative image analysis further allows the maximum level of information to be obtained from super-resolution images, in an objective manner. The combination of super-resolution imaging and quantitative analysis provides a tool for direct comparison with the macroscopic properties of a sample.

### *3.2. Dynamic Moisture Loss*

Figure 2 shows the cumulative moisture loss from the four acid skim milk gels over time. There are clear and reproducible differences between the four sample types and there is a trend that appears to show increased moisture binding with severity of processing history (RHSM >RSM >FHSM

>FSM). This method was developed in order to have a relatively simple and quick way of assessing the water holding capacity of a gel or other soft solid material where moisture binding may be of interest. An aim was to minimise the number of potential driving forces for moisture expulsion from the material. Comparable methods introduce external forces either through centrifugation, capillary forces when material is left on filter paper to drain or undergo greater evaporative losses when experiments are conducted over longer periods under refrigerated conditions. In this instance the gel is in contact with an inert material, and subjected only to gravity. There is likely an increase in surface area of the gel due to the gel forming within the hole of the sieve, but as this is the same for all samples, relative differences between sample type can still be taken into account. The driving forces behind the moisture loss in these experiments is thought to be a combination of drainage of the liquid through the gel network and expulsion of moisture from the gel as it coarsens and contracts with time (Lucey et al., 1998b), increasing the degree of protein-protein interactions. The method employed here has provided a consistent and effective method of monitoring dynamic moisture loss in soft solids.

### *3.3. Macroscopic properties and Rheology*

Figure 3 shows the rheological behaviours of the four acid skim milk gels over time from the gel point. There are large differences between elastic and viscous modulii of the fresh and reconstituted samples, where the reconstituted samples have a higher elastic and viscous modulii. A notable observation from figure 3c is the distinct difference in profile of the tan$\delta$ (the ratio of the viscous to elastic components of the complex modulus). The FSM

| Parameter | Unit | FSM | FHSM | RSM | RHSM |
|---|---|---|---|---|---|
| Final Moisture Loss | % | 42.53 ± 0.65 | 31.78 ± 0.68 | 30.00 ± 0.65 | 25.21 ± 0.51 |
| Degree of Protein Denaturation | % | 17.75 ± 1.5 | 88.75 ± 7.42 | 61.83 ± 13.86 | 95.38 ± 3.34 |
| Yield Stress | Pa | 44.37 ± 7.17 | 2.94 ± 1.40 | 62.98 ± 2.40 | 25.60 ± 5.84 |
| Yield Strain | % | 124.47 ± 8.14 | 20.22 ± 2.31 | 45.56 ± 5.29 | 20.94 ± 1.42 |
| Young's Modulus | $N/m^2$ | 85.25 ± 13.74 | 51.26 ± 11.05 | 170.50 ± 19.91 | 98.00 ± 15.43 |
| Conductivity start | $mS/cm$ | 5.72 ± 0.02 | 5.39 ± 0.05 | 6.44 ± 0.03 | 6.53 ± 0.17 |
| Conductivity end | $mS/cm$ | 6.96 ± 0.10 | 6.96 ± 0.06 | 8.19 ± 0.03 | 8.21 ± 0.05 |
| Final pH | – | 3.99 ± 0.04 | 3.96 ± 0.04 | 4.19 ± 0.04 | 4.20 ± 0.07 |

Table 2: Table showing data from macroscopic analyses of acid milk gels. FSM - Fresh skim milk, FHSM- fresh heated skim milk, RSM - reconstituted skim milk, RHSM - reconstituted heated skim milk. Mean values are shown ± standard deviation.

curve has a smooth decay, as both its elastic and viscous modulii steadily increase in figures 3a-b. Comparatively the other three samples, which have all undergone more severe thermal processing show a clear structural rearrangement during gelation. Structural rearrangement can be seen for the FHSM, RSM and RHSM in figures 3a-c, with this being most apparent in the tan$\delta$ graph. This further supports the fact that there are clear differences between the fresh sample and the other three, a trend which is observable across different physical parameters and different length scales presented here. Table 2 details of the macroscopic properties of the four milk gel samples, highlighting the demonstrable differences in the samples that have occurred due to differences in processing history. Table 2 shows that the FSM has the lowest degree of denatured $\beta$-lg, which is statistically significantly different to the other three samples ($p< 0.05$).

The degree of denatured $\beta$-lg is a key parameter when considering moisture binding in dairy gels. It has been established that denaturing the $\beta$-lg

leads to complexes with the casein micelle and other $\beta$-lg molecules, and increases the moisture binding capacity of a gel. The effect of denatured whey protein on moisture binding is observable when comparing figure 2 with the data in table 2, although the level of denatured $\beta$-lg is not an exact predictor of the final degree of water binding. The two heated samples FHSM and RSM have the highest levels of denatured $\beta$-lg, and are the only pairwise comparison of samples that do not exhibit statistically significant differences ($p< 0.05$). As expected from the pre-concentration and spray drying the RSM has a greater level of denatured $\beta$-lg compared to the FSM.

The RSM had the highest yield stress so can be considered the strongest of the gels, the FHSM being the weakest this was parameter varied significantly ($p< 0.05$) between all four samples. The FSM had the highest yield strain, meaning it was the most deformable under shear. Both the heated samples FHSM and RHSM have similar non-significantly different ($p> 0.05$) yield strain, which seems to compare to the fact both have comparably high levels of denatured $\beta$-lg in them. All other pairwise comparisons of yield strain values are significantly different ($p< 0.05$).

The Young's modulus determined by compression as opposed to the oscillatory shear measurements used to determine the elastic component of the complex modulus shows different trends, meaning the type of deformation applied to these sample types is of importance when considering their physical response. In this case the RSM had the highest Young's modulus, the FHSM being the least elastic, which corroborates with it having the lowest yield stress.

There is a notable and significant difference ($p< 0.05$) in conductivity

between the fresh and reconstituted samples, which could relate to how the minerals are distributed in the fresh and reconstituted systems. Despite the fact that the skim milk powder should contain all the mineral content of the skim milk, there remains a difference in how these minerals are distributed in the final reconstituted sample. For all samples the conductivity increases following acidification and gelation. There will be an increase in the ionic content due to the dissociation of the GDL with time. Under acidic condition the calcium bound within the casein micelles in calcium phosphate nano-clusters is displaced by protons, and therefore the calcium phosphate nano-clusters are depleted from within the micelle. These nano-clusters act as junction points between casein molecules and provide structural integrity to the micelle. Depletion of these junction points leads to changes in the mechanical properties of the micelles themselves as they lose structural integrity, and therefore of any network where they comprise the base level building blocks. This is likely to contribute to the fact that the level of denatured whey protein is not a perfect predictor of alterations to the mechanical properties, as the nature of the casein micelles will be altered by changes to the mineral balance. It is probable that changes in the calcium equilibriums within the sample between free serum $Ca^{2+}$,$Ca^{2+}$ bound to protein and calcium bound in calcium phosphate nano-clusters may play an important role in determining the final mechanical properties of a gel.

There are statistically significant differences between the pH values of fresh and reconstituted samples ($p< 0.05$). However, these differences are not sufficient to expect that differences seen in the physical properties of the samples is due to a differences in pH.

### *3.4. Microstructure*

Figure 4 shows the output from quantitative 2D spatial autocorrelation analysis on the four milk gel samples. It can be seen in figure 4a that there are clear differences between the distribution of $\xi$ values, which correspond to difference in the typical length of the protein structures in the images. This supports the qualitative observations drawn from figure 1 that the FSM sample had larger structural features in comparison to the other samples, which is significantly different to the three other samples ($p< 0.05$). The distributions of the inter-pore distance $\lambda$, shown in figure 4b, differ between the four samples, with the FSM sample being shifted to slightly higher values, supporting the fact that the microstructure was more coarse, with larger structures and larger distance between pores but this parameter did not vary significantly. The fractal dimension of the four samples does not vary greatly, figure 4c, in this case the smallest values for the fractal dimension are in the FSM sample, larger values of $D_f$ being attributed to rougher protein interfaces, or increased surface areas (Smoczyński and Baranowska, 2014). The differences in surface area appear to play a key role in determining the moisture binding in these gel samples, shown in figure 2. The relationship between moisture binding and surface area has been explored further using FLIM measurements and quantitative analysis of the FLIM images.

### *3.5. FLIM Imaging and Image analysis*

Figure 5 shows a representative example of a FLIM image overlayed with an intensity image, where a molecular rotor probe has been used, the fluorescent lifetime of which, depends on the local viscosity. In the lifetime

image, a higher intensity of magenta corresponds to a lower weighted lifetime value. If the molecular rotor were to become attached to, or tightly associated with the protein and network, its number of degrees of freedom would be confined, and this would affect the fluorescent lifetime of the probe. The lifetime of the probe has a non-linear behaviour in fresh milk, compared to viscosity standards as the lifetime values in fresh liquid milk are higher than would be expected based solely on the bulk viscosity of the milk. Therefore the recorded lifetime of the probe in instances where its movement has become confined is likely to relate non-linearly to any absolute viscosity. The magenta image has been produced by fitting a two-component exponential model to the lifetime values in each pixel and establishing a weighted lifetime in each pixel, to which an inverted colourmap has been applied. The lifetime image has then been overlayed with the photon count image, which having been acquired through 2-photon excitation, gives a optically sectioned image, similar to one acquired with confocal microscopy. It is apparent from the overlayed image that the area in closest proximity to the protein structures has a higher intensity in the inverted lifetime image, in effect looking like there is a brighter 'halo' around the protein structures, which in turn suggests that in these regions the ability of the probe to move is different in these regions to within the pores. Moving away from the protein structures into void spaces this intensity decreases, suggesting that further from the protein domains the probe is interacting differently with the surrounding solution. It is proposed that when moving away from a protein structure into a pore there is a typical distance at which water will be initially tightly bound to the protein, and then organised due to the protein-aqueous phase

interface, and then further away will behave like milk serum. This could also be related to there being an ill-defined interface between the protein and aqueous phase, whereas the transition in lifetime between an oil-droplet and aqueous phase is sharp (data not shown).

The pairs of FLIM and intensity images are extremely complex, and it would be extremely difficult to deduce any discerning conclusions from qualitative observations. Quantitative analysis has been applied to these images to extract relevant physical parameters that might aid in explaining the physical behaviours of these samples at a macroscopic scale. Firstly a 2D cross-correlation has been run between the pairs of FLIM images and the intensity images, the cross-correlation image has been radially averaged and fit with a stretched exponential model to extract a typical decay length. The decay length extracted from the cross-correlation corresponds to the typical distance from the protein structures, that there is some change in fluorescent lifetime, effectively measuring the length of the 'halo' in the FLIM image from the protein. The typical length that is extracted from the cross-correlation is termed the binding distance, and is interpreted as a the distance over which the probe's movement is confined due to the presence of the protein shown in figure 6a. If all the gel samples had identical microstructure morphologies it might be expected that moisture binding would relate linearly to the binding distance extracted from the cross-correlation analysis. However, it has been established above that the four samples do exhibit different microstructures, and therefore the actual situation is more complex. Therefore, the perimeter of the protein structures has been determined from the binarised intensity images, figure 6b, the results of which correlate with the average $D_f$ val-

ues for each sample type, indicating surface area and $D_f$ are indeed related. The typical binding distance in each image was multiplied with the total perimeter from the same image to give a binding area in the image, figure 6c.

For all the samples that have undergone more thermal treatment, FHSM, RSM and RHSM the trend in binding area, shown in figure 6c correlate with the trend seen in dynamic moisture loss. For these three samples that are morphologically more similar, and have all shown similar behaviours during gel formation (figure 3) the effective binding area of the protein network can be used to explain differences in the dynamic moisture loss of these samples, demonstrating the potential that FLIM imaging and quantitative analysis has in exploring and understanding soft solids and food at the micro-scale that can provide understanding of the physical properties on the macro-scale. The results from the FSM do not correlate with its level of moisture loss, but it has been established that this sample has behaved quite differently to those having undergone more severe heat treatment.

### *3.6. Dynamic moisture loss vs structure*

The experiments conducted in this study highlight that alterations in process history can have significant effects on the final physical properties of a acid skim milk gel, from the nano to macro-scale. The ability of an acid milk gel to hold water is an important quality in a final product, and this has been assessed through a novel methodology to track the dynamic water loss of a sample. Clear differences were observed between all samples, showing a direct effect of heat treatment prior to gelation, and between the use of fresh or reconstituted skim milk.

An initial hypothesis might have suggested that dairy samples that had undergone a greater degree of thermal processing would bind more water. Greater thermal processing would lead to an increased amount of denatured whey protein, in particular $\beta$-lg, which has a high water binding capacity. Denatured $\beta$-lg can bind the $\kappa$-casein as both has a free thiol group, allowing the formation of a di-sulphide bond, which can lead to dimerisation of $\beta$-lg too (Corredig and Dalgleish, 1996; Nair et al., 2013). In theory the greater the level of bound whey proteins to the casein network, the greater the water binding capacity of the gel as a whole. It can be seen in table 2 that this theory does not fully explain the moisture loss data shown in figure 2. Investigation into the microstructure of the gel using super-resolution STED imaging and quantitative image analysis has shown that the different gel samples have different morphologies, figures 1 & 4. Microstructural analysis showed that the FSM sample tended to have larger protein domains with greater distances between pores, indicating a coarser structure.

The presence of denatured $\beta$-lg at the surface of the casein micelles in the heated samples might offer an explanation as to why morphological differences in the gel structures can be observed in the microscopy images and quantified in the image analysis. $\beta$-lg has a higher iso-electric point compared to casein, 5.2 and 4.6 respectively (Reithel and Kelly, 1971; Anema, 1998). During gel formation the pH will have been below the pI of the whey proteins, which may then have become slightly positively charged. As gel formation between the casein micelles is mediated by the fact that they are at their iso-electric point, and patches on the micelles that had charged $\beta$-lg covalently bound to them may have been less likely to participate in intra-

molecular bonding upon collision and interaction, leading to thinner strands in the gel compared to the more coarse FSM, where coarser structures have a lower protein surface area.

The presence of denatured $\beta$-lg associated with the casein micelles has been shown to increase the $G'$ of acid milk gels. The change in mechanical properties has been explained by there being more protein participating in the gel network, therefore more interaction points between micelles and micelle aggregates, increasing the elastic component of the complex modulus (Lucey et al., 1998b; van Vliet et al., 2004; Bikker, Anema, Li, and Hill, 2000). An increase in gel firmness in gels produced from reconstituted skim milk powders have been attributed to whey protein denaturation that has occurred during powder production (Lucey et al., 1998b). Differences in macroscopic properties and water binding are likely to have been affected by the altered mineral balance, determined through changes in conductivity, depletion off calcium phosphate nano-clusters has been shown to affect the type of gel formed and degree of moisture binding (Loveday et al., 2013).

The relationship between microstructure and moisture binding was further explored through the use of a rotary molecular probe that is sensitive to the local viscosity in a material. The use of rotary probes to monitor food quality is currently being explored and has a fascinating potential to contribute to monitoring foods over their shelf life, and could contribute to tackling global food waste (Alhassawi et al., 2018). We have demonstrated herein, that it is possible to utilise the approach of monitoring viscosity and water activity in a bulk spectroscopic manner, and conduct this experiment with a microscope to spatially resolve this information within a complex col-

loidal food system. Rotary probes could be used to provude valuable new information compared to the bulk approach as it would not only be possible to track when changes occur over a products life, but where these changes are occurring in the microstructure of the food, whether it is a composite soft solid material or a tissue structure. The combination of FLIM imaging and image analysis have provided greater insights into how moisture is bound in acid milk gels and has shown for milk samples that have more than 50 % denatured $\beta$-lg the overall ability of a gel to hold water is strongly correlated with the effective area around the protein where the molecular movement of the aqueous phase is confined.

Correlation between the different variables assessed does not provide a definitive link between structure and rheology or moisture binding, however the microscopy experiments conducted in this study require small samples, with very minimal sample preparation, imaging can be performed rapidly and the image analysis can be automated. If sufficient correlations can be drawn between precise microstructural features, microscopy could act as an effective screening tool, particularly with the advent of increasingly intelligent robots and big data processing. In future the screening of many sample/product formulations could be automated with the most appropriate selected based on microstructure, without having to do exhaustive and time consuming rheological testing on all the samples. Similarly, screening for changes in microstructural differences between a fresh and reconstituted sample may allow for optimisation in the sample/product production to either minimise differences between the two, or to explore novel structures and product properties that can be achieved with different raw materials.

## 4. Conclusions

A range of methodologies has been presented to better investigate acid milk gels on different length scales, capable of not only measuring the macroscopic rheology and elastic modulus but dynamic moisture loss, without exposing the sample to external force. Quantified FLIM images show how the molecular confinement changes spatially across a samples microstructure. Quantitative image analysis of STED images enables microstructures to be differentiated from each other and described using precise physical parameters. A range of analytical techniques has been applied to four gel samples, produced from fresh or reconstituted skim milk, with either no heat treatment or a heat treatment. The thermal processing history of skim milk samples affects the final microstructure and macroscopic properties of acid induced gels. The alterations in microstructure and macroscopic properties are not easily disentangled from one another, nor predicted from a single measurement, but the ensemble of analytical tools presented herein, gives a comprehensive overview of the processes occurring on varying length scales in a complex colloidal food material, from the size of the protein domains and inter-pore distance, fractal dimension, protein surface area, area of water confinement in the microstructure, dynamic moisture loss, rheological properties pH, conductivity and protein chemical analysis. A more severe thermal history can lead to clear changes in moisture binding, rheological properties and microstructure which is not solely explained by the level of denatured whey protein. Differences in conductivity indicate clear differences between the mineral balance of fresh and reconstituted milk gels, the effects of which will be explored in future works.

## Acknowledgements

The authors acknowledge the Danish Molecular Biomedical Imaging Center (DaMBIC, University of Southern Denmark) for the use of the bioimaging facilities. This work was funded by Arla Foods a.m.b.a., Denmark.

## Competing interest statement

The authors have no competing interests.

## References

## References

Ako, K., Durand, D., Nicolai, T., Becu, L., 2009. Quantitative analysis of confocal laser scanning microscopy images of heat-set globular protein gels. Food Hydrocolloids 23 (4), 1111–1119.

Alhassawi, F. M., Corradini, M. G., Rogers, M. A., Ludescher, R. D., 2018. Potential applications of luminescent molecular rotors in food science and engineering. Critical reviews in food science and nutrition 58 (11), 1902–1916.

AlKanhal, H. A., Abu-Lehia, I. H., Al-Saleh, A. A., 1994. Changes in the quality of fresh and recombined ultra high temperature treated milk during storage. International Dairy Journal 4 (3), 221–236.

Amatayakul, T., Sherkat, F., Shah, N. P., 2006. Syneresis in set yogurt as affected by eps starter cultures and levels of solids. International Journal of Dairy Technology 59 (3), 216–221.

Anema, S. G., 1998. Effect of milk concentration on heat-induced, ph-dependent dissociation of casein from micelles in reconstituted skim milk at temperatures between 20 and 120 c. Journal of Agricultural and Food Chemistry 46 (6), 2299–2305.

Auty, M., O'Kennedy, B., Allan-Wojtas, P., Mulvihill, D., 2005. The application of microscopy and rheology to study the effect of milk salt concentration on the structure of acidified micellar casein systems. Food Hydrocolloids 19 (1), 101–109.

Auty, M. A., Twomey, M., Guinee, T. P., Mulvihill, D. M., 2001. Development and application of confocal scanning laser microscopy methods for studying the distribution of fat and protein in selected dairy products. Journal of Dairy Research 68 (03), 417–427.

Bikker, J. F., Anema, S. G., Li, Y., Hill, J. P., 2000. Rheological properties of acid gels prepared from heated milk fortified with whey protein mixtures containing the a, b and c variants of $\beta$-lactoglobulin. International Dairy Journal 10 (10), 723–732.

Busko, D., Baluschev, S., Crespy, D., Turshatov, A., Landfester, K., 2012. New possibilities for materials science with sted microscopy. Micron 43 (5), 583–588.

Corredig, M., Dalgleish, D. G., 1996. Effect of temperature and ph on the interactions of whey proteins with casein micelles in skim milk. Food Research International 29 (1), 49–55.

Glover, Z. J., Ersch, C., Andersen, U., Holmes, M. J., Povey, M. J., Brewer, J. R., Simonsen, A. C., 2019b. Super-resolution microscopy and empirically validated autocorrelation image analysis discriminates microstructures of dairy derived gels. Food Hydrocolloids 90, 62–71.

Glover, Z. J., Bisgaard, A. H., Andersen, U., Povey, M. J., Brewer, J. R., Simonsen, A. C., 2019a. Cross-correlation analysis to quantify relative spatial distributions of fat and protein in super-resolution microscopy images of dairy gels. Food Hydrocolloids 97, 105225.

Haidekker, M. A., Theodorakis, E. A., 2007. Molecular rotors—fluorescent biosensors for viscosity and flow. Organic & Biomolecular Chemistry 5 (11), 1669–1678.

Hell, S. W., 2003. Toward fluorescence nanoscopy. Nature biotechnology 21 (11), 1347.

Hell, S. W., 2008. Microscopy and its focal switch. Nature methods 6 (1), 24.

Hell, S. W., Wichmann, J., 1994. Breaking the diffraction resolution limit by stimulated emission: stimulated-emission-depletion fluorescence microscopy. Optics letters 19 (11), 780–782.

Krop, E. M., Hetherington, M. M., Holmes, M., Miquel, S., Sarkar, A., 2019. On relating rheology and oral tribology to sensory properties in hydrogels. Food Hydrocolloids 88, 101–113.

Kuimova, M. K., 2012. Mapping viscosity in cells using molecular rotors. Physical Chemistry Chemical Physics 14 (37), 12671–12686.

Kuimova, M. K., Botchway, S. W., Parker, A. W., Balaz, M., Collins, H. A., Anderson, H. L., Suhling, K., Ogilby, P. R., 2009. Imaging intracellular viscosity of a single cell during photoinduced cell death. Nature chemistry 1 (1), 69.

Kuimova, M. K., Yahioglu, G., Levitt, J. A., Suhling, K., 2008. Molecular rotor measures viscosity of live cells via fluorescence lifetime imaging. Journal of the American Chemical Society 130 (21), 6672–6673.

Laguna, L., Farrell, G., Bryant, M., Morina, A., Sarkar, A., 2017. Relating rheology and tribology of commercial dairy colloids to sensory perception. Food & function 8 (2), 563–573.

Levitt, J. A., Kuimova, M. K., Yahioglu, G., Chung, P.-H., Suhling, K., Phillips, D., 2009. Membrane-bound molecular rotors measure viscosity in live cells via fluorescence lifetime imaging. The Journal of Physical Chemistry C 113 (27), 11634–11642.

Loveday, S. M., Sarkar, A., Singh, H., 2013. Innovative yoghurts: Novel processing technologies for improving acid milk gel texture. Trends in food science & technology 33 (1), 5–20.

Lucey, J., Munro, P., Singh, H., 1998a. Rheological properties and microstructure of acid milk gels as affected by fat content and heat treatment. Journal of Food Science 63 (4), 660–664.

Lucey, J., Munro, P., Singh, H., 1999. Effects of heat treatment and whey protein addition on the rheological properties and structure of acid skim milk gels. International Dairy Journal 9 (3), 275–279.

Lucey, J. A., Tamehana, M., Singh, H., Munro, P. A., 1998b. Effect of interactions between denatured whey proteins and casein micelles on the formation and rheological properties of acid skim milk gels. Journal of Dairy Research 65 (4), 555–567.

Lucey, J. A., Teo, C. T., Munro, P. A., Singh, H., 1998c. Microstructure, permeability and appearance of acid gels made from heated skim milk. Food Hydrocolloids 12 (2), 159–165.

Ludescher, R. D., Peting, L., Hudson, S., Hudson, B., 1987. Time-resolved fluorescence anisotropy for systems with lifetime and dynamic heterogeneity. Biophysical chemistry 28 (1), 59–75.

Marangoni, A. G., Acevedo, N., Maleky, F., Peyronel, F., Mazzanti, G., Quinn, B., Pink, D., et al., 2012. Structure and functionality of edible fats. Soft Matter 8 (5), 1275–1300.

Mezzenga, R., Schurtenberger, P., Burbidge, A., Michel, M., 2005. Understanding foods as soft materials. Nature materials 4 (10), 729.

Nair, P. K., Dalgleish, D. G., Corredig, M., 2013. Colloidal properties of concentrated heated milk. Soft Matter 9 (14), 3815–3824.

Reithel, F., Kelly, M. J., 1971. Thermodynamic analysis of the monomer-dimer association of. beta.-lactoglobulin a at the isoelectric point. Biochemistry 10 (13), 2639–2644.

Robertson, C., George, S. C., 2012. Theory and practical recommendations for autocorrelation-based image correlation spectroscopy. Journal of biomedical optics 17 (8), 080801.

Smoczyński, M., Baranowska, M., 2014. A fractal approach to microstructural changes during the storage of yoghurts prepared with starter cultures producing exopolysaccharides. Journal of texture studies 45 (2), 121–129.

Strasburg, G. M., Ludescher, R. D., 1995. Theory and applications of fluorescence spectroscopy in food research. Trends in Food Science & Technology 6 (3), 69–75.

Super, B. J., Bovik, A. C., 1991. Localized measurement of image fractal dimension using gabor filters. Journal of visual communication and image representation 2 (2), 114–128.

Urbonaite, V., De Jongh, H., Van Der Linden, E., Pouvreau, L., 2015. Water holding of soy protein gels is set by coarseness, modulated by calcium binding, rather than gel stiffness. Food hydrocolloids 46, 103–111.

Urbonaite, V., van der Kaaij, S., de Jongh, H., Scholten, E., Ako, K., van der Linden, E., Pouvreau, L., 2016. Relation between gel stiffness and water holding for coarse and fine-stranded protein gels. Food Hydrocolloids 56, 334–343.

van Vliet, T., Lakemond, C. M., Visschers, R. W., 2004. Rheology and structure of milk protein gels. Current Opinion in Colloid & Interface Science 9 (5), 298–304.

Vasbinder, A. J., Alting, A. C., Visschers, R. W., de Kruif, C. G., 2003. Texture of acid milk gels: formation of disulfide cross-links during acidification. International Dairy Journal 13 (1), 29–38.

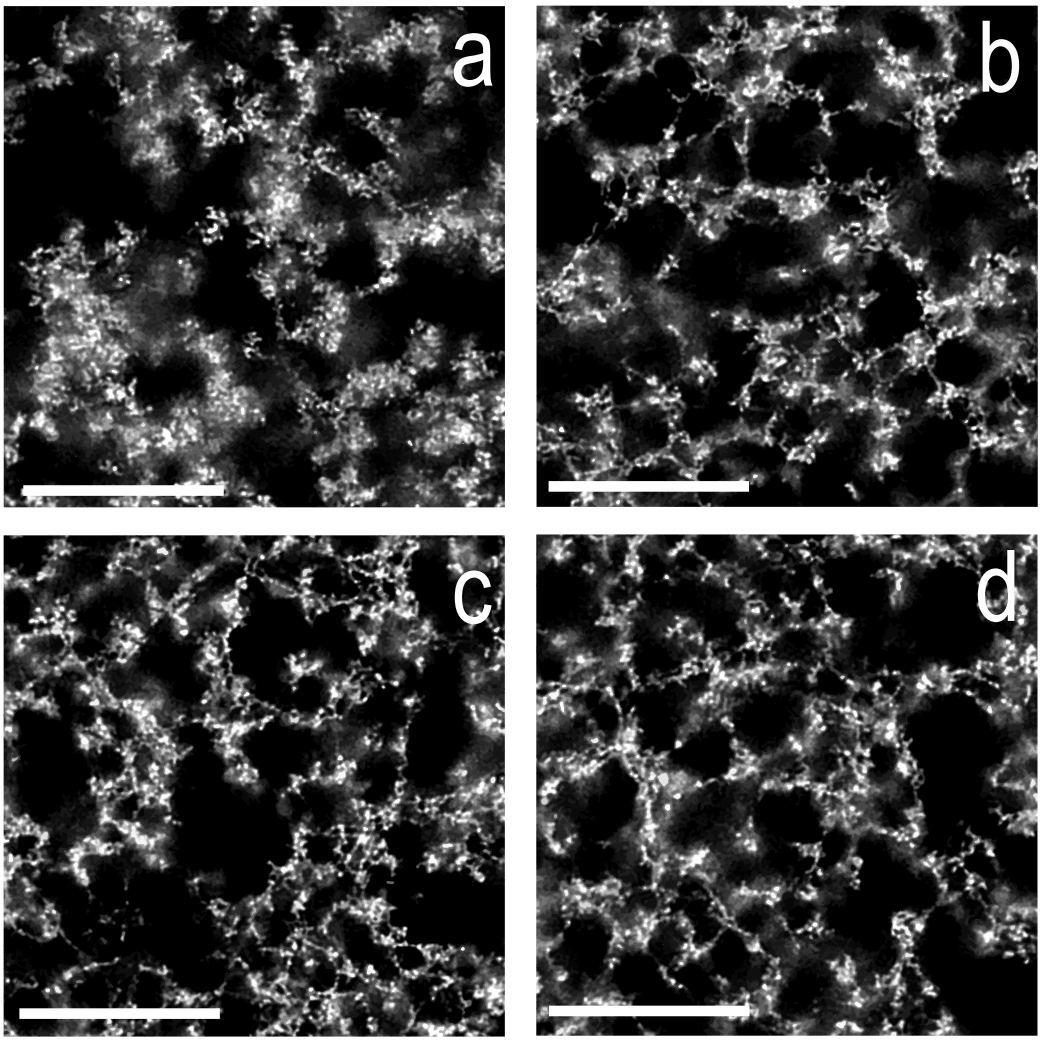


Figure 1: Typical STED microscopy images of the acid induced skim milk gel samples under investigation. Fresh skim milk (a). Fresh heated skim milk (b). Reconstituted skim milk (c). Reconstituted heated skim milk (d). All imaged after 90 minutes after acid addition at 35 °C. Scalebar 10 $\mu$m.

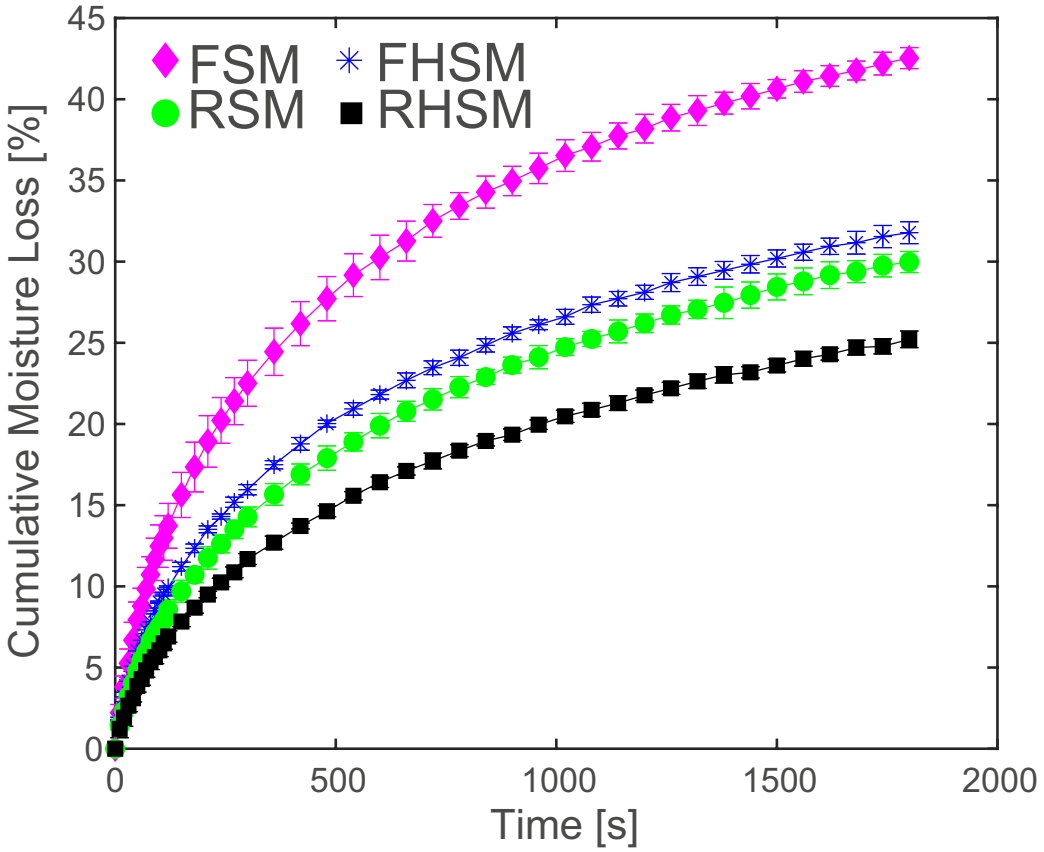


Figure 2: Cumulative moisture loss over time of acid induced skim milk gels under investigation, time zero is 90 minutes after acid addition at 35 °C. Error bars show the standard error of the mean.

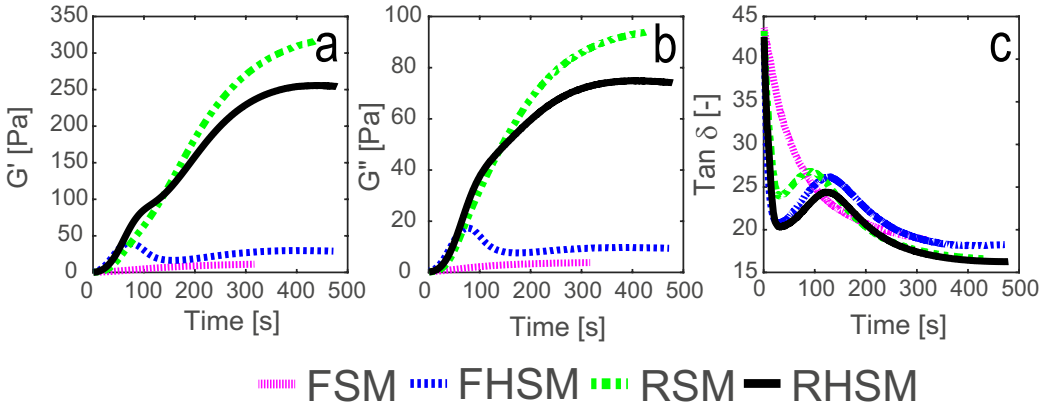


Figure 3: Rheology of acid skim milk gels over time, following acid addition. Elastic component of the complex modulus $G'$ (a). Viscous component of the complex modulus $G''$ (b). Ratio of $G''$ to $G'$, tan$\delta$ (c).

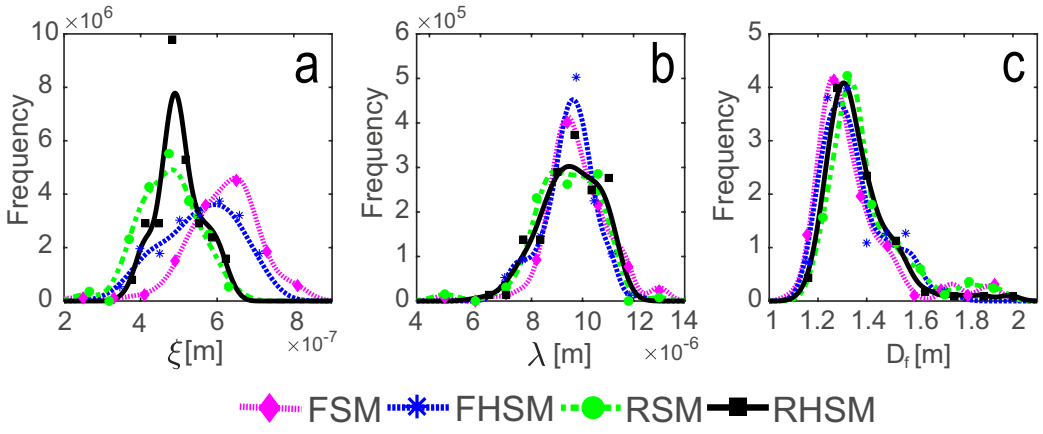


Figure 4: Output from image analysis of STED microscopy images of acid induced skim milk gels. Typical length of protein domains in the gel, $\xi$, (a). Inter-pore distance, $\lambda$ (b). Fractal Dimension, $D_f$ (c).

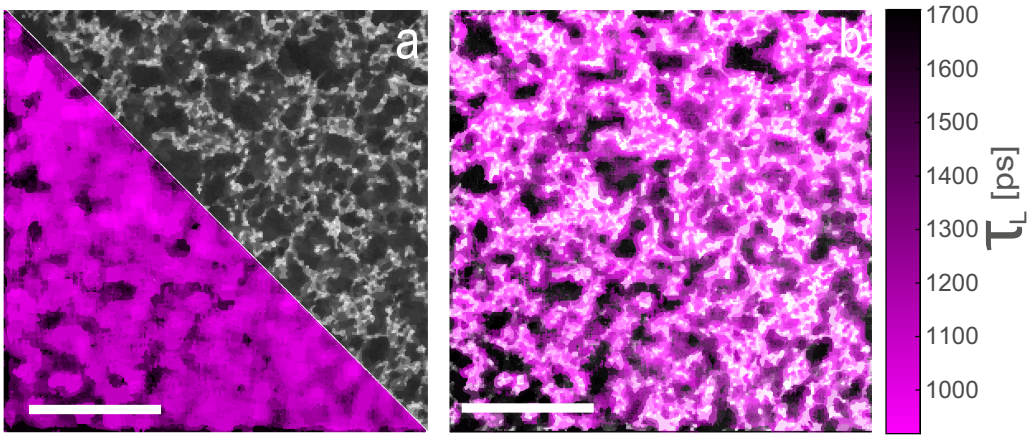


Figure 5: Spatially resolved micro-viscosity measurements acquired using FLIM imaging of an image of fresh heated acid skim milk gel. Higher intensity of magenta relates to lower fluorescent lifetime values. Diagonally sliced images showing the lifetime image in magenta and the intensity image in greyscale (a). Overlay of the lifetime image and the intensity image (b). Colourbar indicated weighted fluorescent lifetime values from model fitting. Scalebar 10 $\mu$m.

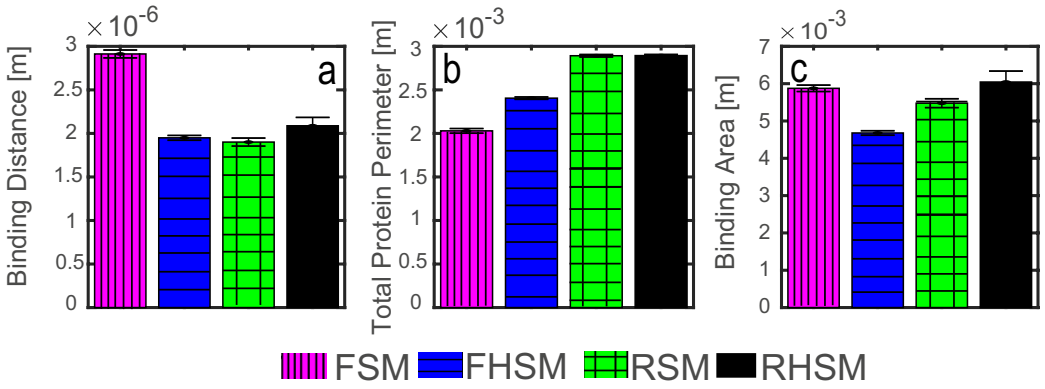


Figure 6: Output from image analysis of the FLIM images. Binding distance derived from the decay length of the radially averaged cross-correlation decay between the lifetime and intensity images, showing the typical distance where the molecular movement of the aqueous phase is affected by the protein network (a). Total perimeter calculated from the binarised intensity image (b). Binding area in an image determined from the product of the binding distance and perimeter values (c). Errorbars show the standard error of the mean